JOURNAL OF PROPULSION AND POWER
Vol. 11, No. 3, May–June 1995

Thrust Vectoring Control from Convergent Nozzles with Translating Side Wall

Kenneth C. Cornelius* and Gerald A. Lucius†
Wright State University, Dayton, Ohio 45435

Experimental measurements of side force for an underexpanded two-dimensional nozzle and an axisymmetric contraction for a three-dimensional nozzle with side wall translation demonstrate that vectored angles of 20 deg can be obtained at a pressure ratio of 11.5. For a vectored control jet the magnitude of side force can be increased by the translation of the side wall where the optimum length is dependent on the pressure ratio value. The inviscid wave equation results are in good agreement with the experimental two-dimensional measurements. The optimum length of extension for the three-dimensional nozzle occurs at 1.6 times the throat dimension with similar thrust vectoring capability. The physics of the expansion and the jet momentum turning are qualitatively described using an optical schlieren system.

Nomenclature

A^*	=	linear dimension of throat 0.1 cm for two-dimensional nozzle
C_d	=	discharge coefficient
D_i	=	three-dimensional nozzle throat diameter, 0.5 cm
F_t	=	isentropic force
F_x	=	axial force
F_y	=	side force
F_{ym}	=	maximum side force
H	=	height dimension of nozzle wall
I, II	=	right and left running waves
k	=	ratio of specific heats
L_x	=	total length of side wall extension
M	=	Mach number $V/(kRT)^{0.5}$
M^*	=	Mach number based on T^*
$\dot{m}$	=	nozzle mass flow rate
P_a	=	atmospheric pressure
P_r	=	pressure ratio, P_0/P_a
P_0	=	total plenum pressure
P^*	=	nozzle throat pressure
R	=	ideal gas constant
R_d	=	Reynolds number based on D_i, 1.44×10^5
T^*	=	throat temperature
V	=	velocity
(X, Y)	=	coordinate axis
θ	=	momentum vector angle
θ_s	=	streamline angle from horizontal
ν_{pe}	=	Prandtl-Meyer expansion angle
ρ	=	density of air
ω	=	angle that defines origin of II family

Introduction

RECENT investigations of the propulsion system with variable exhaust nozzle geometry show increased aircraft performance using vectored thrust in the pitch and yaw axes. The effects of different nozzle designs on the internal performance including nonsymmetric, single ramp expansion, and wedge flap to provide thrust vectoring have been investigated.[1–8] The emphasis was to provide two degrees of freedom in the pitch and yaw axes for thrust vectoring with minimum weight and complexity of hardware design. The translation of the side wall referred to single expansion ramp nozzles (SERN) was first reported[6] to produce a side force from the expansion of the flow from the open side. The resulting yaw vector angle for this method was increased for configurations where the expansion area ratio for the two-dimensional nozzle was decreased. The maximum yaw vector angle was 8.0 deg at $P_r = 10$ with the side wall removed entirely showing a nonlinear trend with the side wall length. These results were for a nozzle with an aspect ratio of 3.67 and with a small area ratio of 1.08. The total thrust loss was minimal for the optimum configuration. The deflection of flaps in both sidewalls produced the largest yaw vector angle. Simultaneous pitch and yaw vectors were achieved with an external downstream flap for the pitch axis where the total force decreased due to pressure drag on the flap configurations associated with the turning. With rotating external flaps, yaw angles of 20 deg were attained. However, this technique was not amenable to thrust vectoring from two axes simultaneously.

The approach in this research was to examine the maximum side force that could be obtained from the translating side wall concept using the simple geometry of an underexpanded nozzle. The extension of the bottom and side wall provided for the nonsymmetric supersonic expansion of the flow for a two- and three-dimensional nozzle geometry to provide two-axes thrust vectoring. The focus of this study was to examine the basic physics of the supersonic expansion for these nozzles and to experimentally measure and compare the magnitude of the side force to the axial force at different P_r values. From this data the optimum wall extension for maximum thrust has been determined for these nozzle geometries.

Approximate One-Dimensional Theory and Two-Dimensional Compressible Wave Equation

One-Dimensional Theory

In an attempt to quantify the limit of the side force magnitude possible for the extension of the side wall, a comparison was made between the converging nozzle thrust ratio to the maximum thrust for a gas in which the thermodynamic variables behave according to the ideal gas relationship.

The upper limit of the magnitude of the side force was assessed through the examination of the one-dimensional gas-dynamic force or thrust equation. A force ratio was defined

Presented as Paper 93-3261 at the AIAA Shear Flow Conference, Orlando, FL, July 6–9, 1993; received Sept. 4, 1993; revision received Sept. 9, 1994; accepted for publication Sept. 14, 1994.

*Associate Professor, Department of Mechanical and Materials Engineering. Senior Member AIAA.
†Graduate Student. Member AIAA.

by dividing the F_t of a converging-diverging nozzle by the isentropic F_x due to a converging nozzle. The theoretical result[9] was for the full expansion to atmospheric pressure, which provides for the hypothetical maximum side force for a fixed P_r when the expansion occurs on one side wall:

$$\frac{F_t}{F_x} = \frac{k\left[\left(\frac{2}{k-1}\right)\left(\frac{2}{k+1}\right)^{(k+1)/(k-1)}\right]^{1/2}\left[1-\left(\frac{P_a}{P_0}\right)^{(k-1)/k}\right]^{1/2}}{2\left(\frac{2}{k+1}\right)^{1/(k-1)} - \frac{P_a}{P_0}} \tag{1}$$

The total force can be represented in terms of the vector contributions of axial and side force, where $F_t^2 = F_x^2 + F_y^2$. The vector diagram of the forces results in the following equation for the ratio of the side to axial force:

$$F_y/F_x = [(F_t/F_x)^2 - 1]^{1/2} \tag{2}$$

This value represents the upper limit of possible side force and is a unique function of P_r. The one-dimensional equation results were used as a guideline for the two-dimensional supersonic flow results. The maximum turning angle from the vectored momentum of the jet θ is defined from the vector diagram of the force ratio:

$$\tan(\theta) = F_y/F_x \tag{3}$$

The analytical expression in Eq. (2) represents the hypothetical maximum of F_y/F_x, which increases monotonically with P_r. The two-dimensional experimental data will be lower than this value from the propagation of the expansion and compression waves throughout the supersonic flowfield.

Two-Dimensional Wave Equation

The inviscid wave equation is the proper mathematical model that produces a side force that will be lower than the one-dimensional analytical expression from Eqs. (1–3). Figure 1 shows a sketch of the basic physics of the expansion and compression waves in the supersonic region of an underexpanded nozzle. High-pressure air passes through the throat at a pressure of P^* and $M = 1$, whereupon the flow expands supersonically downstream between the area defined by the solid boundary and the outer shear layer. For an underexpanded nozzle, the pressure decreases downstream from P^* at the throat from the supersonic expansion to the local atmospheric pressure. Due to the nature of the supersonic compressible gasdynamic wave equation, the flow expands and then contracts as the expansion waves reflect off the shear layer as compressive waves. A numerical model utilizing the inviscid two-dimensional wave equation was solved using the method of characteristics to evaluate the nondimensional parameter P/P^*, and the results integrated to provide for the side force. The side force is generated when the P_r becomes greater than critical, i.e., for $P_r > [2/(k+1)]^{-k/(k-1)}$, and increases with P_r. The flow can be considered to be an isentropic expansion to the local static pressure, which neglects the surface shear stress and the turbulent shear interface along the outer streamline. At the exit of the underexpanded nozzle the flow streamline that defines the outer shear layer turns abruptly at the corner to the Prandtl-Meyer expansion angle expressed as

$$\nu_{pe} = \sqrt{[(k+1)/(k-1)]}\tan^{-1} \times \sqrt{[(k-1)/(k+1)](M^2-1)} - \tan^{-1}\sqrt{M^2-1} \tag{4}$$

For isentropic flow the Mach number can be expressed in terms of the local pressure ratio as

$$M^2 = [2/(k-1)][(P/P_0)^{(1-k)/k} - 1] \tag{5}$$

Along this streamline the flow is supersonic and the flow is fully expanded to atmospheric pressure. As the P_r increases, both the shear layer angle ν_{pe} and the corresponding Mach number increase. The Prandtl-Meyer expansion around the upper corner produces a point source for the expansion waves that emanate from the singularity. The numerical results used a procedure based on the lattice point technique with wave increments at 0.25 deg.[9] Figure 2 shows the hodograph plane where M^* and θ are the polar coordinates that demonstrate the expansion and compression process as waves from family *I* intersect and cross waves of family *II*. The waves reflect from the solid surface as expansion waves that then impinge on the shear layer. The mechanics of the reflection of the waves from the shear layer result in the formation of compressive waves to satisfy the boundary condition of constant pressure along this streamline. Simultaneously, the outer shear layer turns toward the surface downstream that reduces the shear layer angle to maintain a constant Mach number along the streamline.[9] The inviscid wave equation is an accurate model for the supersonic expansion on a solid wall of a finite length where disturbances from downstream cannot propagate upstream. The flow transitions through an oblique shock that originates at the end of the solid wall to satisfy the boundary conditions. The jet momentum is vectored to the angle θ defined in Eq. (3) to satisfy the integral momentum equation. The F_x remains constant for this problem. The F_y is the net result of the pressure integration from the exit plane at P^* to P_a along the length of the sidewall. The maximum side force on the wall occurs when the Mach number is fully expanded to atmospheric pressure along the streamline adjacent to the

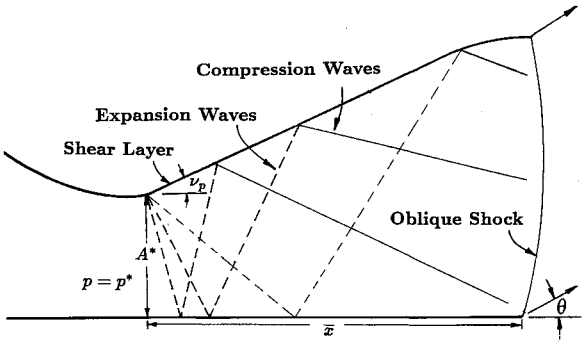

Fig. 1 Basic physics for thrust vectoring.

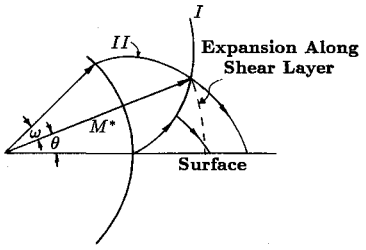

Fig. 2 Sketch of hodograph plane.

solid boundary. The optimum length that produces the maximum side force will be a function of the P_r.

Experimental Arrangement

The thrust vectoring for an underexpanded nozzle was examined experimentally to highlight the physics and ascertain the magnitude of the side force. The axial and the side forces were measured for variable wall extension on each nozzle configuration. Figure 3 shows the experimental arrangement for two-dimensional thrust vectoring. A calibrated two-component force transducer was utilized for the measurement of the side and axial forces. In both measurements, tares were removed to access the corrected values of the side and axial forces. The compressed air line connected to a plenum that had a converging nozzle with a slot height of 0.1 cm and width of 2.0 cm, which provided for an aspect ratio of 20 for the jet. Side walls were designed and connected to the sides of the contraction to achieve a higher effective aspect ratio. The plenum was machined into a dovetail traverse to facilitate the extension of the bottom wall relative to the exit plane of the nozzle. This provided a range of extensions of the bottom straight wall for the measurement of the side force at different P_r values. Using a calibrated venturi the C_d was measured as 0.94 at $P_r = 2.0$ and increased to 0.95 at $P_r = 11$ for the two-dimensional nozzle. Pressure transducers were used for the plenum total pressure and measurement of the wall static pressure and were calibrated using a standard pressure source. A barometer was used for the measurement of the local atmospheric pressure. The parameter x/A^*, which represents the nondimensional extension of the bottom wall, was varied from a value of 0 to the limit at $x/A^* = 13$. This experimental procedure was followed for each P_r. A monochromatic light source with associated optics was utilized for a schlieren system. This technique was used for qualitative flow visualization using photographs of the density gradients produced in the supersonic regime of the nozzle expansion flowfield.

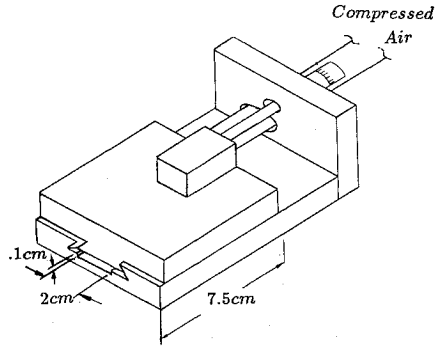

Fig. 3 Experimental arrangement for two-dimensional thrust vectoring.

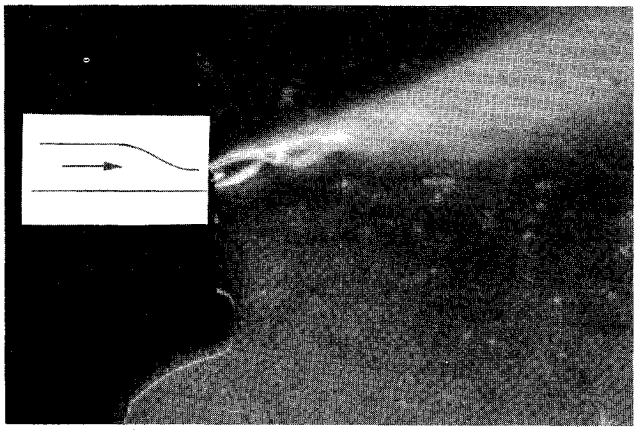

Fig. 4 Photograph of supersonic region.

Experimental Results

Two-Dimensional Nozzle

Schlieren photographs in Fig. 4 show that at $P_r = 7.5$ an oblique shock forms within 2.0 slot heights at the end of the solid wall extension, whereupon the flow turns through an angle relative to the x-axis, which is normal to the jet exit plane. This photograph clearly shows the compression and expansion waves characteristic of an underexpanded jet and the transition to the strong oblique shock with the departure of the jet from the surface. As P_r increases, the shear layer angle also increases, which provides for a self-adjusting expansion that is contained between the solid boundary and the shear layer. The data of normalized surface pressure P/P^* is presented in Fig. 5 for various P_r values. The curves nearly coalesce when plotted using the normalizing value of the throat pressure. The two-dimensional inviscid wave equation results of the axial surface pressure P/P^* are also plotted in Fig. 5. Figure 6 shows the measured maximum side force ratio with the bottom wall extension X_l adjusted to provide for the maximum force ratio F_{ym}/F_x vs P_r, including a comparison to the two-dimensional wave numerical results. Figure 6 shows a thrust vectored angle of 20 deg was obtained experimentally at a $P_r = 11.5$. The theoretical results were obtained from the integration of the pressure evaluated along the solid boundary from the exit plane to the normalized atmospheric pressure defined as $P_a/P^* = [2/(k+1)]^{k/(k-1)}/P_r$. Figure 7 shows the side force variation vs the downstream extension of the wall x/A^* at different P_r values. The optimized length vs P_r for the maximum side force is shown in Fig. 8 for the two-dimensional nozzle. This graph also includes the thrust vectored angle θ from the horizontal plane. Figure 9 shows the normalized side force F_y/F_{ym} distribution vs X/A^* at various P_r values, which demonstrates that a large percentage of the side force is generated for wall lengths less than the maximum asymptotic value in the range of $X/A^* \sim 2.0$.

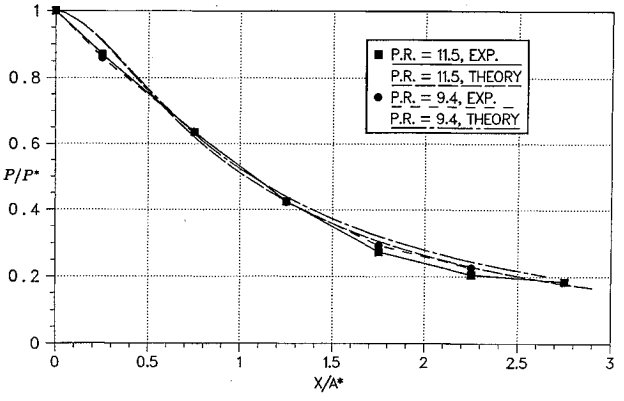

Fig. 5 Measured P/P^* distribution vs X/A^* for two-dimensional thrust vectoring.

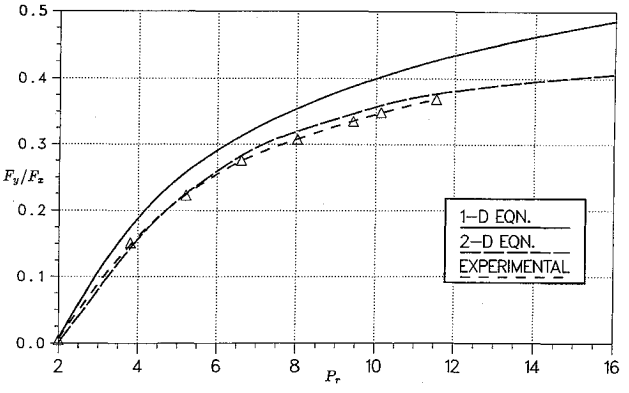

Fig. 6 Maximum side force ratio F_{ym}/F_x vs P_r.

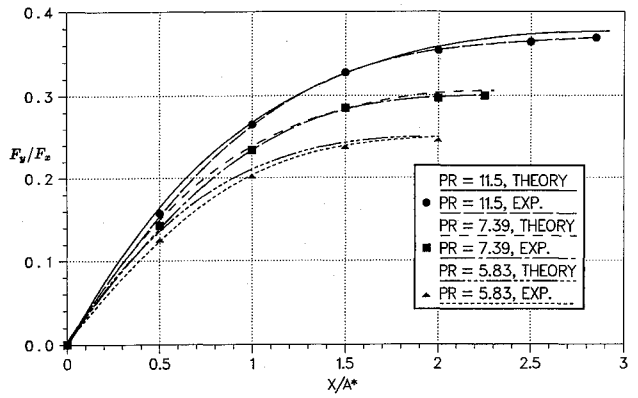

Fig. 7 F_y/F_x vs x/A^* at various P_r for two-dimensional nozzle.

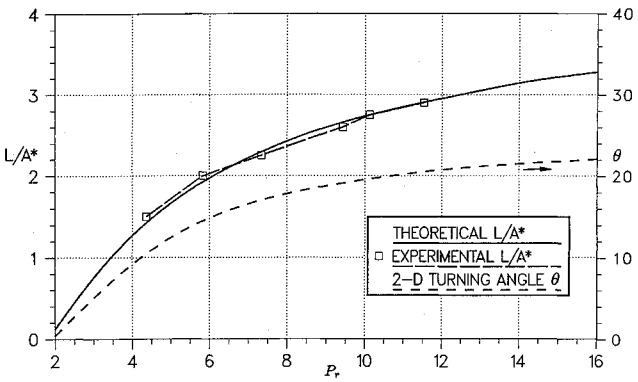

Fig. 8 Wall length for maximum side force and vector angle.

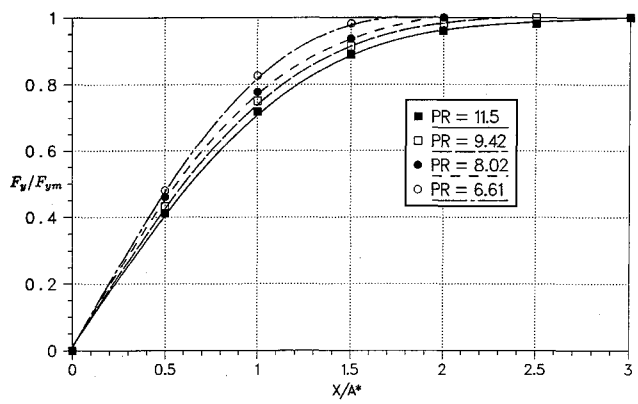

Fig. 9 Side force ratio F_y/F_{ym} vs x/A^*.

Figure 10 represents a plot of the outer shear layer coordinates for the underexpanded nozzle from the numerical results at different P_r. The length of the shear layer when the curves asymptote represents the half wavelength of the supersonic expansion before the wave pattern repeats as the compressive waves converge downstream. This length is much greater than the length for the optimum side force as the flow overexpands downstream until the wave mechanics at the shear layer interface are satisfied. Figure 11 is a plot of the experimental data of the force ratio farther downstream. The data demonstrate that the side force approaches a minimum below zero and then increases due to the physics of the wave equation. The experimental results for higher P_r show an increase in the overall wavelength with the dissipation of energy. The entropy increase is attributed to the reflections of the waves from the time-varying shear layer that translate to fluctuations of both velocity and density. The correlation of the flow variables produces a time-averaged turbulence pro-

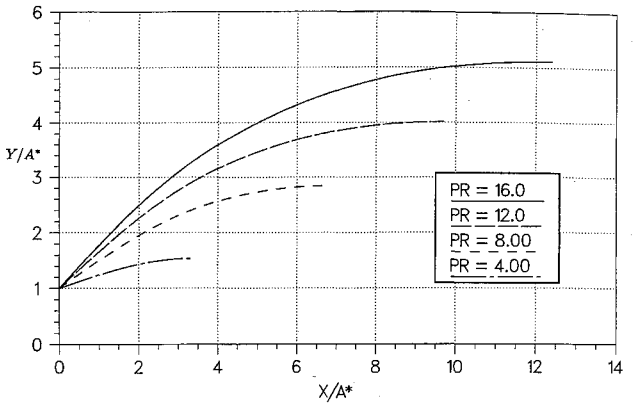

Fig. 10 Outer shear layer coordinates for underexpanded nozzle.

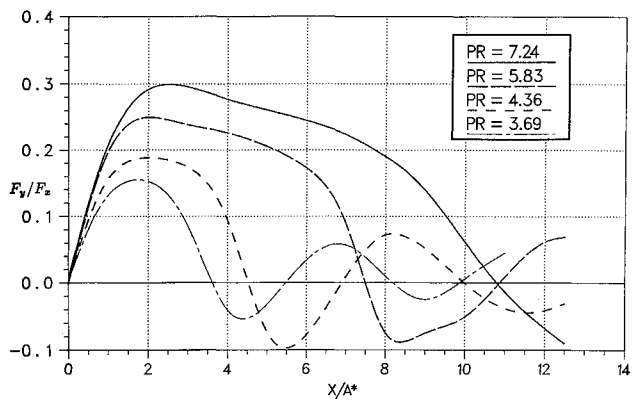

Fig. 11 F_y/F_x vs x/A^* at various P_r for two-dimensional nozzle.

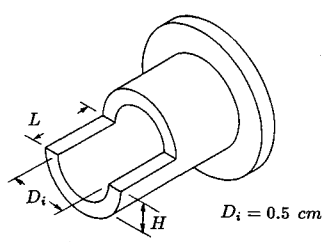

Fig. 12 Schematic of experimental three-dimensional nozzle.

duction throughout the entire jet domain. Most of the entropy effects occur downstream as the compressive waves are reflected from the shear layer. This feature of the flow physics has a negligible impact on the thrust vectoring results.

Three-Dimensional Nozzle

Figure 12 shows a schematic diagram of the experimental three-dimensional nozzle. This nozzle has an axisymmetric contraction to the throat diameter of $D_i = 0.5$ cm. The upper wall was machined to a fixed height of $H/D_i = 0.78$ to provide for the Prandtl-Meyer expansion of the flow along this plane. The height dimension was measured relative to the i.d., where preliminary experimental results showed that this H/D_i value produced the maximum side force. Three separate nozzles were tested with different side wall extensions defined by L/D_i, ranging from 1.4 to 2.0. Figure 13 shows a schlieren photograph of the supersonic expansion of the three-dimensional nozzle. Figure 14 represents a sketch of the physics of the three-dimensional expansion downstream. The vortex sheet coalesces into two vortices that stretch the jet in the horizontal direction. A laser light sheet using small seed particles as the scattering media produced a cross-sectional view of the boundary of the jet. Figure 15 shows the photographic com-

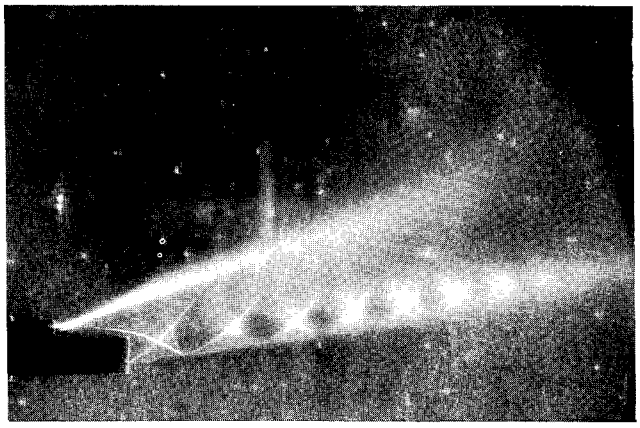

Fig. 13 Schlieren photograph of supersonic expansion.

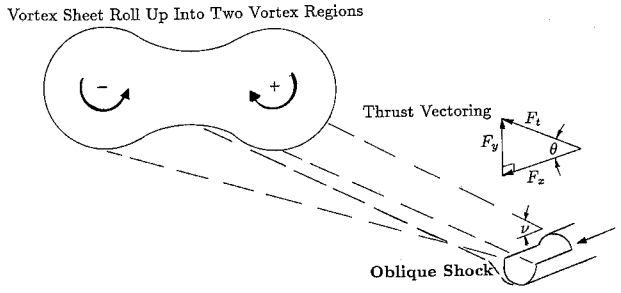

Fig. 14 Physics of three-dimensional expansion downstream.

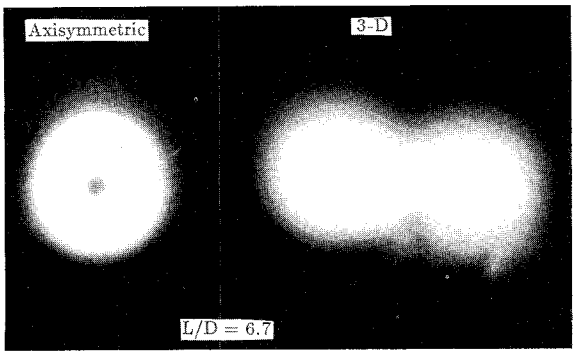

Fig. 15 Laser light sheet comparison at $X/D_i = 6.7$, $P_r = 7.5$.

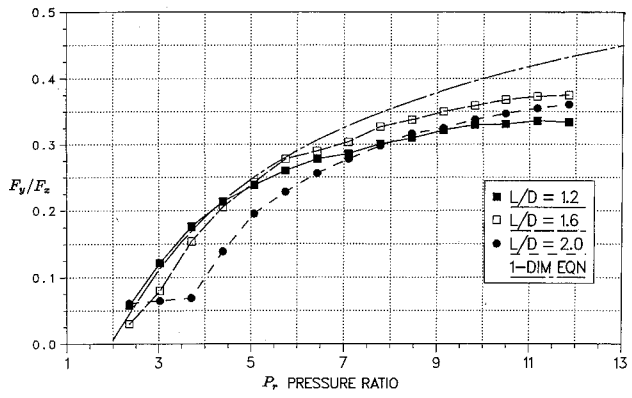

Fig. 16 F_y/F_x vs P_r for three-dimensional nozzle.

parison, when viewed down the x axis, of an axisymmetric nozzle flow to the three-dimensional nozzle flowfield at the downstream location of $X/D_i = 12$ and $P_r = 7.5$. Using this qualitative optical technique, the flow structure that emanates from the three-dimensional nozzle has greater entrainment by virtue of the vortex sheet dynamics. The vortex sheet roll-up from the bottom surface increases the turbulent interface between the vortical and nonvortical fluid. Figure 16 represents the measured data for F_y/F_x vs P_r for the three-dimensional nozzle configuration for three separate fixed wall extensions. This plot includes the comparison to the isentropic analytical expression from Eqs. (1–3), which was derived using the axial and side force contributions to the total thrust vector. Unlike the two-dimensional results where the wall length increases with a P_r increase, the optimum wall length was $L/D_i = 1.6$ at the higher P_r values. This was attributed to the complex three-dimensional flow expansion from this geometry.

Conclusions

The simple geometry of an underexpanded jet with wall extension shows that a large percentage of thrust vector can be recovered from the flow expansion on the side wall. An experiment was undertaken to measure the thrust vectoring capability from an underexpanded nozzle with a side wall extension. The asymmetry of the expansion was produced by an extension of one side wall. Excellent agreement was obtained between the two-dimensional inviscid wave equation results and the corresponding experimental data. For the two-dimensional nozzle the optimum length increases monotonically with P_r for the two-dimensional nozzle. Thrust vectoring angles of the order of 20 deg at $Pr = 11$ were obtained by an extension of the side wall in the range of $2.0A^*$. The magnitude of F_y/F_x was greater for the three-dimensional nozzle with optimum wall length of $L/D_i = 1.6$ at the higher P_r values. This was an unexpected result and attributed to the complex three-dimensional physics of the expansion process from this geometry, although the basic physics are similar to the two-dimensional flow expansion problem. The data demonstrate that for both the two- and three-dimensional nozzles a large magnitude in side force can be obtained from the geometric extension of the side wall, where the thrust vectoring angle increases with P_r. The total force from these nozzles approaches the isentropic one-dimensional force to within 2% at a P_r of 11.0 from a calculation of the F_y deficit contribution from the theoretical maximum. This loss would be added to the conventional losses of skin friction and boundary-layer growth that was measured as 5% for the nozzles tested. This result demonstrates the efficient turning for this configuration. The difference between the one-dimensional thrust equation and the total thrust measured increases with P_r and is entirely due to the inviscid expansion and compression wave propagation that is inherent in the solution of the wave equation. For the three-dimensional nozzle, vectored thrust can be produced in other quadrants by having a segmented arrangement around the periphery to exercise wall translation in the desired plane. Another mode of operation would be to rotate the downstream slotted segment of the nozzle to provide for pitch and yaw capability. This technique can be utilized for multiaxes thrust vectoring that has merit for a remotely piloted vehicle and cruise missile applications.

Acknowledgment

Support for this research is acknowledged from the Wright State University Research Incentive funds.

References

[1]Capone, F. J., "The Nonaxisymmetric Nozzle—It is for Real," AIAA Paper 79-1810, Aug. 1979.

[2]Re, R. J., and Leavitt, L. D., "Static Internal Performance Including Thrust Vectoring and Reversing of Two-Dimensional Convergent-Divergent Nozzles," NASA TP-2253, 1984.

[3]Re, R. J., and Berrier, B. L., "Static Internal Performance of Single Expansion-Ramp Nozzles with Thrust Vectoring and Reversing," NASA TP-1962, 1982.

[4]Berrier, B. L., and Mason, M. L., "A Static Investigation of Yaw Vectoring Concepts on Two-Dimensional Convergent-Divergent Nozzles," AIAA Paper 83-1288, June 1983.

[5]Stevens, J. L., Thayer, E. B., and Fullerton, J. F., "Development of the Multi-Function 2-D/C-D Nozzle," AIAA Paper 81-1491, July 1981.

[6]Mason, M. L., and Berrier, B. L., "Static Investigation of Several Yaw Vectoring Concepts on Nonaxisymmetric Nozzles," NASA TP-2432, June 1985.

[7]Yetter, J. A., and Leavitt, L. D., "Effects of Sidewall Geometry on the Installed Performance of Nonaxisymmetric Convergent-Divergent Exhaust Nozzles," NASA TP-1771, Dec. 1980.

[8]Berrier, B. L., and Re, R. J., "Effect of Several Geometric Parameters on the Static Internal Performance of Three Nonaxisymmetric Nozzle Concepts," NASA TP-1468, July 1979.

[9]Shapiro, A. H., *The Dynamics and Thermodynamics of Compressible Fluid Flow*, Vol. 1, Wiley, New York, 1953, pp. 450–490.